Cell Stem Cell, Volume *20*

Supplemental Information

Modeling Psychomotor Retardation using iPSCs from MCT8-Deficient Patients Indicates a Prominent Role for the Blood-Brain Barrier

Gad D. Vatine, Abraham Al-Ahmad, Bianca K. Barriga, Soshana Svendsen, Ariel Salim, Leslie Garcia, Veronica J. Garcia, Ritchie Ho, Nur Yucer, Tongcheng Qian, Ryan G. Lim, Jie Wu, Leslie M. Thompson, Weston R. Spivia, Zhaohui Chen, Jennifer Van Eyk, Sean P. Palecek, Samuel Refetoff, Eric V. Shusta, and Clive N. Svendsen

Supplemental Information

Supplementary Figures

Supplementary Figure 1.

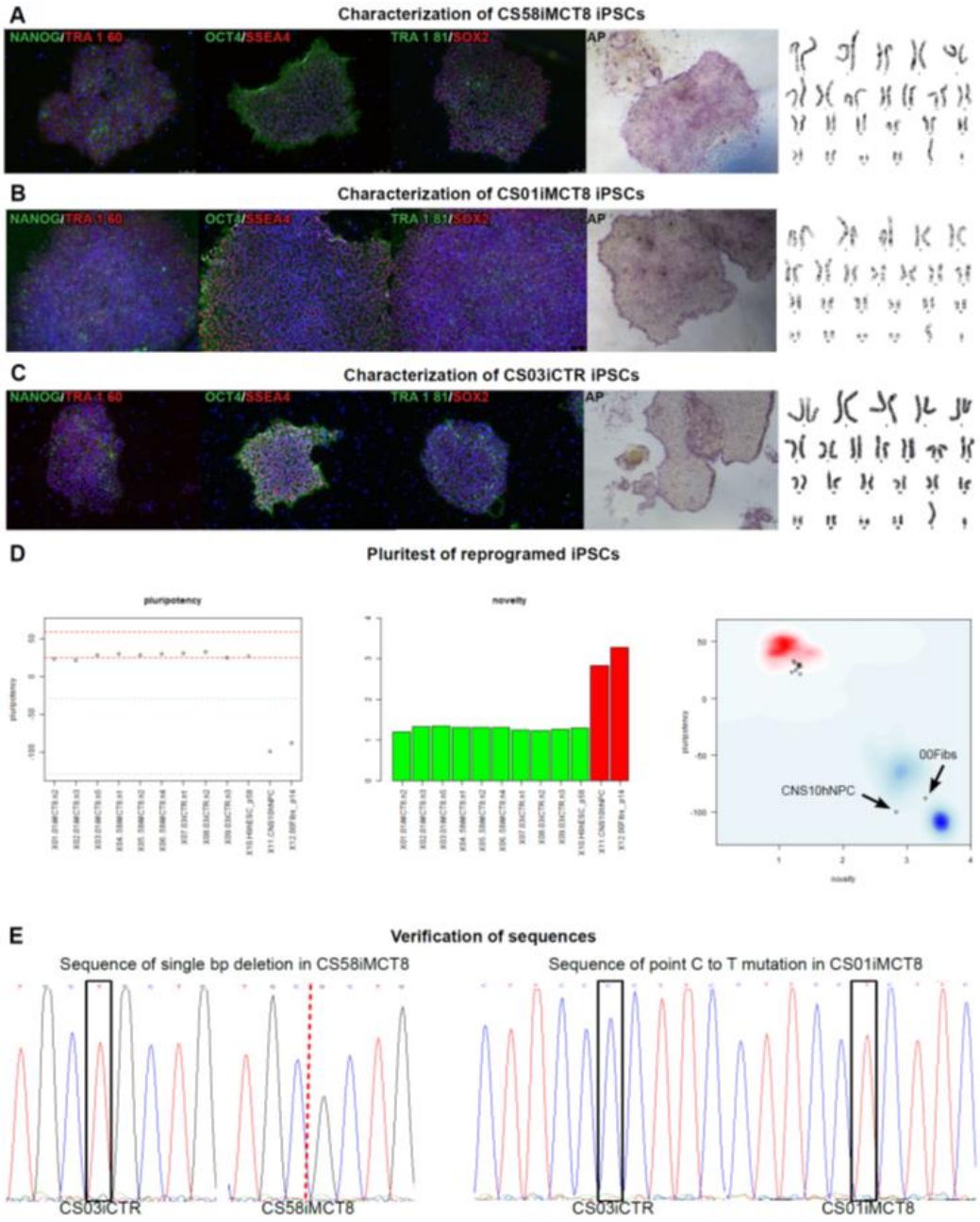

Supplementary Figure 2.

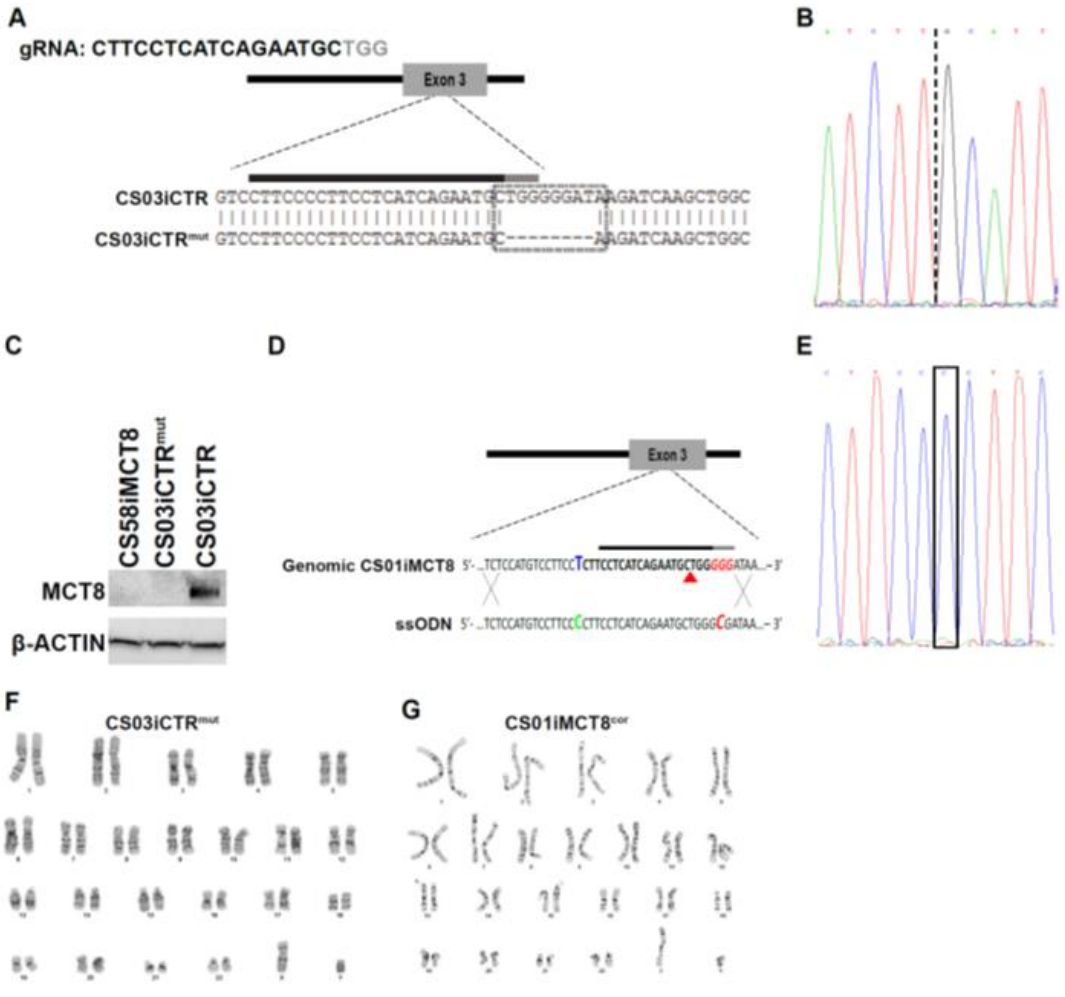

Supplementary Figure 3

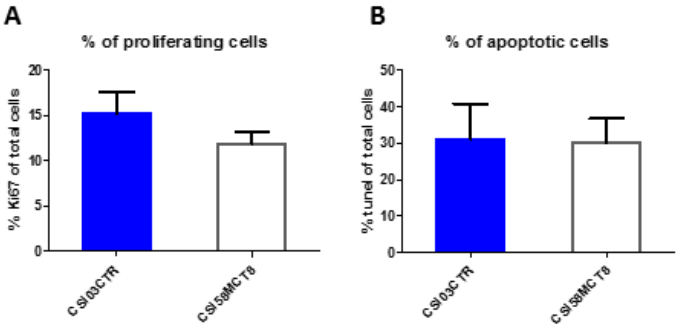

Supplementary Figure 4.

A

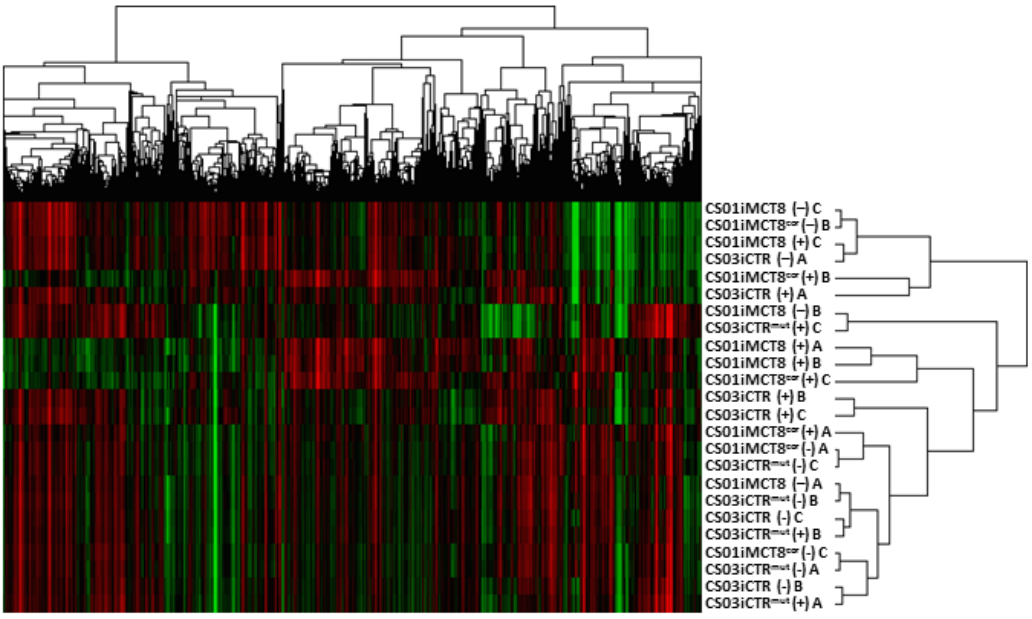

B

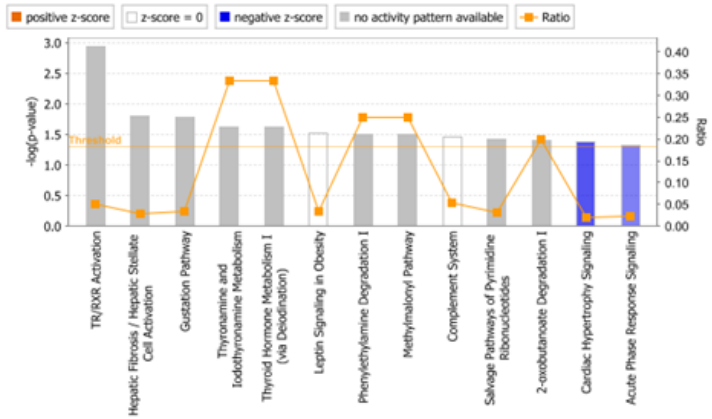

Supplementary Figure 5.

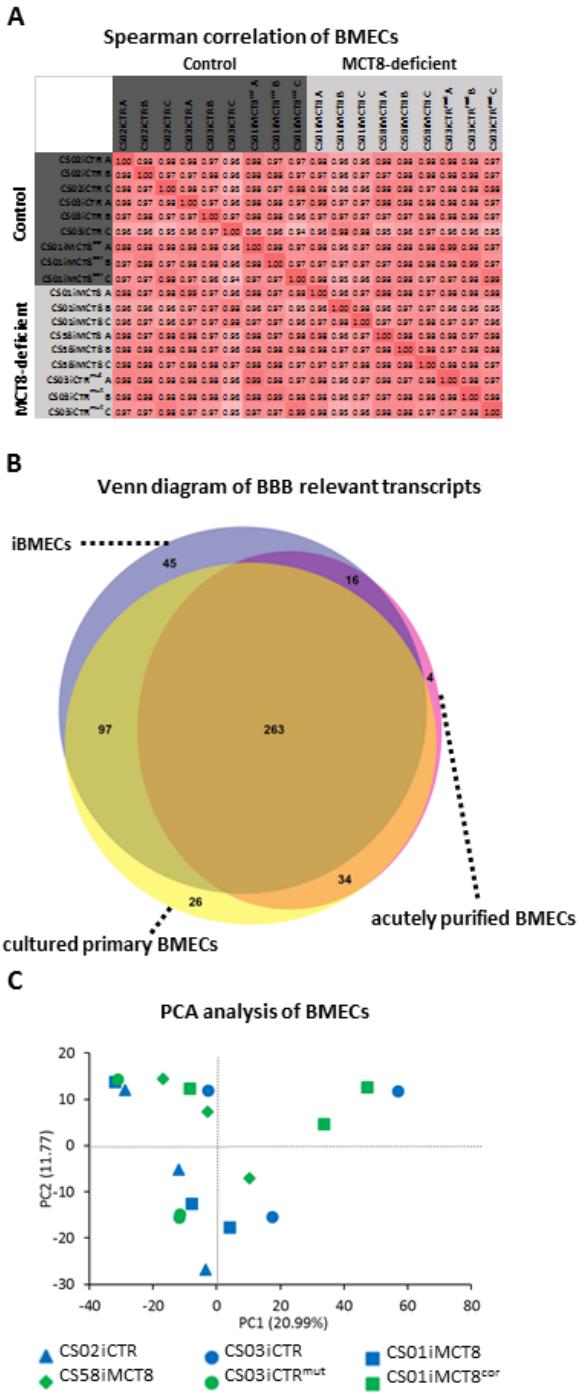

Supplementary Figure 6.

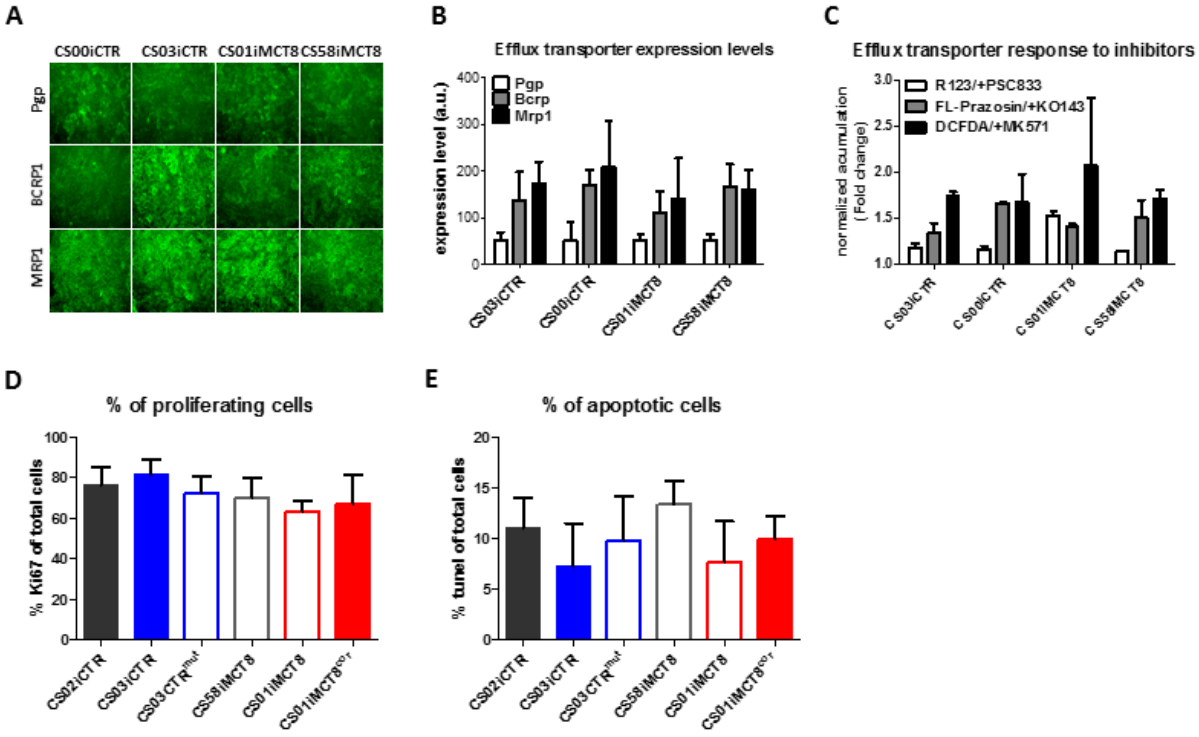

Supplementary Figure 7.

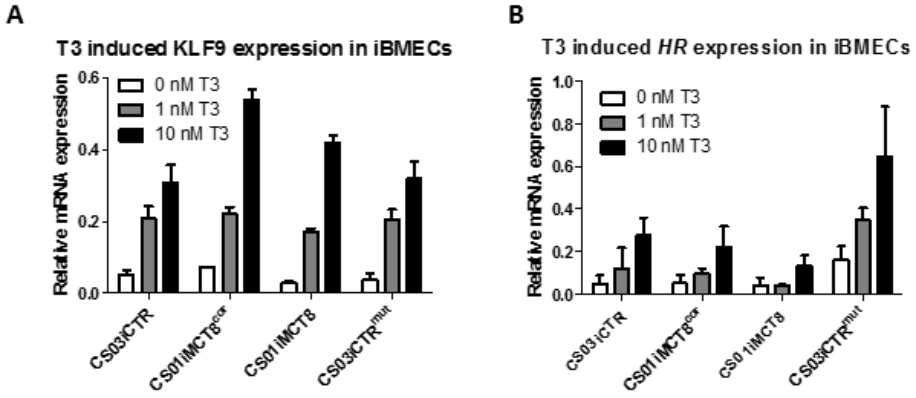

Supplementary Figure legends

Supplementary Figure 1. Related to Figure 1 and STAR methods. Generation and characterization of iPSCs from MCT8-deficient patients and associated healthy controls. Fibroblasts from MCT8-deficient patients 2558, 4601 and the healthy control 4603 (father of 4601) were reprogramed into iPSCs using non-integrating episomal plasmids. Three clones from each iPSC line were chosen and used for all experiments. A-C) Characterization of representative clones by immunocytochemistry for the pluripotency markers NANOG/TRA160, OCT4/SSEA4 and TRA181/SOX2, as well as Alkaline phosphatase (AP) activity and karyotype analysis. D) Pluritest of reprogramed iPSCs. Pluripotency score (left panel), novelty score (middle panel) and a combination of both pluripotency and novelty score (right panel). A fibroblast line (00Fibs) and human neural progenitor cells (CNS10hNPC) were used as references. E) Validation of the mutation sequence in the *MCT8* gene was verified in the CS58iMCT8 line and in the CS01iMCT8 line.

Supplementary Figure 2. Related to Figure 1 and STAR methods. Generation and characterization of isogenic cell lines. A) Guide RNA (gRNA) sequence of the Cas9 construct and its location within exon3 of the *MCT8* (*SLC16A2*) gene. Grey nucleotides represent the PAM sequence (NGG). Sequence alignment shows an 8 base pair deletion generated by the Cas9/CRISPR system on the background of the CS03iCTR line resulting in the CS03iCTR^{mut} line. B) Electropherograms showing the location of the 8 base pair deletion in the CS03iCTR^{mut} line. C) Western blot analysis of the MCT8 protein. β-Actin was used as a reference protein. D) Schematic of the Cas9/CRISPR-mediated homologous recombination procedure for correcting the point mutation in the CS01iMCT8 line in order to generate the CS01iMCT8^{cor} isogenic line. Single-stranded donor oligonucleotide (ssODN) was used as a template for homology directed

repair (HDR). This sequence includes the T to C (green) as well as a silent C to G mutation in the pam sequence. E) Electropherograms showing the corrected T to C sequence resulting in the CS01iMCT8^{cor} isogenic line that contains a sequence that translates to a functional MCT8 protein on the background of the CS01iMCT8 cell line. G-band karyotype analysis reveals no abnormalities caused by the gene editing process in the F) CS03iCTR^{mut} and G) CS01iMCT8^{cor} isogenic lines.

Supplementary Figure 3. Related to Figure 1. Proliferation and apoptosis in neural cells. A) The percent of proliferating cells was assessed by counting the number of cells expressing Ki67 out of total Dapi-labeled cells. No significant differences were observed between control (CS03iCTR) and MCT8-deficient (CS58iMCT8) cells. B) The percent of apoptotic cells was assessed by a Tunel assay. No significant differences were observed between control (CS03iCTR) and MCT8-deficient (CS58iMCT8) cells. Error bars represent SD.

Supplementary Figure 4. Related to Figure 2. Transcriptional profiling of iPSC-derived neural cells. A) Unsupervised hierarchical gene clustering of EZ-spheres differentiated into neural cells for 30 days in the presence (+) or absence (-) of T_3. Uppercase characters represent biological replicates. B) Ingenuity pathway analysis (IPA) on differentially expressed genes suggest pathways that may be involved in T_3 signaling in neural cells.

Supplementary Figure 5. Related to Figure 4. Transcriptional profiling of iBMECs. A) Spearman correlation analysis over total RNA-seq data demonstrates high correlation between control and MCT8-deficient iBMECs datasets. B) Venn diagram comparing BBB-related gene expression of iBMECs (blue), human BMECs acutely purified by immunopanning (pink) (Zhang et al., 2016) and primary cultured human BMECs (Cell Systems, ACBRI 376, yellow). A set of 506 genes was tested for expression in each BMEC source. The gene set included: 20 TJ and

known BBB-related genes (see Table S5) (Bauer et al., 2014; Geier et al., 2013; Huntley et al., 2014; Liebner et al., 2011; Obermeier et al., 2013), *all* 25 CLDN genes, *all* 407 solute carrier (SLC) transporters, and *all* 53 ATP-binding cassette (ABC) transporters. CLDN, SLC and ABC genes were included regardless of *a priori* knowledge of BBB association. Genes expressed in the respective RNA-seq data sets were then included in the analysis. The human BMECs (pink), acutely purified by immonopanning, expressed 317 of the 506 genes. iBMECs (blue) expressed 421 genes including 88% of genes expressed in purified human BMECs. Primary cultured human BMECs (yellow) expressed 420 genes including 93% of genes expressed in purified human BMECs. C) Principal component analysis (PCA) shows no MCT8-dependent clustering in control (blue) and MCT8-deficient (green) iBMECs, and that differences between biological replicates are not greater than the differences across cell lines.

Supplementary Figure 6. Related to Figure 4. Characterization of iBMECs. A) Immunocytochemistry analysis showed the efflux transporters P-glycoprotein (P-gp), breast cancer resistance protein (BCRP) and the multidrug resistance-associated protein 1 (MRP1) in healthy control (CS03iCTR and CSi00CTR) and in MCT8-deficient (CS01iMCT8 and CS58iMCT8) iBMECs (20x magnification). B) "Flow cytometry quantification shows that efflux transporter protein expression is not significantly different between healthy control (CS03iCTR and CSi00CTR) and MCT8-deficient (CS01iMCT8 and CS58iMCT8) groups (ANOVA). C) Assessment of efflux transporter activities in iBMECs presented as fold change in increased accumulation rate of the P-gp substrate rhodamine 123 (R123) in response to the P-gp specific inhibitor PSC833 (white bars), the BCRP substrate prazosin in response to the BCRP inhibitor Ko143 (grey bars) and the MRP family substrate carboxymethyl-2',7'-dichlorofluorescein diacetate (DCFDA) in response to the MRP specific inhibitor MK571 (black bars) shows no

statistically significant differences between healthy control (CS03iCTR and CSi00CTR) and MCT8-deficient (CS01iMCT8 and CS58iMCT8) groups (ANOVA). D) The percent of proliferating iBMECs was assessed by counting the number of cells expressing Ki67 out of total Dapi-labeled cells. No significant differences were observed between functional MCT8 (CS03iCTR, Cs02iCTR and CS01iMCT8^{cor}) lines and MCT8-deficient (CS03iCTR^{mut}, CS58iMCT8 and CS01iMCT8) lines. E) The percent of apoptotic cells was assessed by a Tunel assay. No significant differences were observed between functional MCT8 (CS03iCTR, Cs02iCTR and CS01iMCT8^{cor}) lines and MCT8-deficient (CS03iCTR^{mut}, CS58iMCT8 and CS01iMCT8) lines. Error bars represent SD.

Supplementary Figure 7. Related to Figure 5. T_3-induced gene expression in iBMECs. qRT-PCR analysis of T_3-induced gene expression. A) No significant differences were observed in *Kruppel-like factor 9* (*KLF9*) mRNA levels between functional MCT8 (CS03iCTR, and CS01iMCT8^{cor}) and MCT8-deficient (CS01iMCT8, CS3iCTR^{mut}) iBMECs. B) No significant differences were observed in *Hairless* (*HR*) mRNA levels between functional MCT8 (CS03iCTR, and CS01iMCT8^{cor}) and MCT8-deficient (CS01iMCT8, CS3iCTR^{mut}) iBMECs. Error bars represent SD.

Supplemental Table 1. Related to Figure 1, S1 and STAR methods. Cell background information. Cell line description, mutations ethnicity, gender, age at sampling, clinical characteristics and references.

Cell line	Mutation	Ethnicity	Gender	Age	Clinical characteristics	Reference
CS58iMCT8	A404fs416X	Combined ethnic background including Scottish, English, and Cree Indian	Male	8	Severe psychomotor retardation symptoms and abnormal thyroid parameters	Dumitrescu et al., 2003
CS01iMCT8 and CS01iMCT8^{cor})	P321L	Jewish Ashkenazi	Male	2.5	Severe psychomotor retardation symptoms and abnormal thyroid parameters	Verge et al., 2012
CS03iCTR (and CS03iCTR^{mut})	Control	Jewish Ashkenazi	Male	39	Healthy control, father of CS01iMCT8	
CS00iCTR	Control	African American	Male	6	Healthy control	
CS14iCTR	Control	Unknown	Female	52	Healthy control	
CS02iCTR	Control	Caucasian	Male	52	Healthy control	

Supplemental Table 2. Related to Figure 1, S2 and STAR methods. Off-target mutation analysis. PCR analysis was performed on 10 loci within coding sequences, predicted to share high homology with the MCT8 3rd exon gRNA target to exclude off-target mutations evoked by the gene targeting process.

Gene	Locus	Mismatch positions	Fwd Primer	Rev Primer
NM_006475	chr13:+38160222	4MMs [1:3:7:8]	aatttttccctgcctttgct	gaaacttccacgaggtgtcc
NM_003922	chr15:+64039181	4MMs [3:8:9:10]	tgggacagttgagtccatca	ttggtttcagagaacaccacag
NM_145804	chr11:-34186298	4MMs [2:3:8:13]	gtctcagtgtcctccgtgct	tggctgaagcagttcatgtc
NM_012262	chr1:-87574783	3MMs [5:6:15]	acaccaatttttccccttcc	gcaaattctgtttccaacttga
NM_001142548	chr1:-46743910	4MMs [1:2:10:15]	agccccttttccctatctcc	ccgggatgaggtactccag
NM_198185	chr11:+7722094	4MMs [1:9:10:13]	ttattccggcacatgagtga	ggaattgtgctgggatctgt
NM_014330	chr19:-49376913	4MMs [1:2:7:15]	ctcttcctcggctttctcct	tgatggcatgtatggtgagc
NM_001007471	chr9:-73206077	4MMs [4:5:12:13]	ttgtttctccctctgcttcc	gatgttcttggccagtttcc
NM_001193455	chr5:-6609995	4MMs [2:3:5:16]	tcatctttgcggtatttgtctt	gacgtttattccacggcatt
NM_001143989	chr1:-108779088	4MMs [3:4:15:20]	ctgtgaccacacccttttgtg	gccggtaagagttggacttg
NM_000165.4	chr6:+121768615	4MMs [5:11:12:13]	tggattcagcttgagtgctg	ggtcgctctttcccttaacc

Supplemental Table 3. Related to Figure 2. List of T_3-induced gene expression in healthy control neural cells. Healthy control (CS03iCTR) EZ-spheres were differentiated in the presence and/or absence of T_3 for 32 days. Genes plotted were significantly T_3-induced after multiple comparison correction calculated for 0.1 false discovery rate (FDR) (q-value) and were of 1.5-fold change or more.

Supplemental Table 4. Related to Figure 2. List of T_3-repressed gene expression in healthy control neural cells. Healthy control (CS03iCTR) EZ-spheres were differentiated in the presence

and/or absence of T_3 for 32 days. Genes plotted were significantly T_3-repressed after multiple comparison correction calculated for 0.1 FDR (q-value) and were of 1.5-fold change or more.

Supplemental Table 5. Related to Figure 4 and Figure S5. List of known BBB-related genes. The set of 506 genes used for comparison of human BMEC sources was composed of the 20 TJ and known BBB-related genes listed here as well as 407 solute carrier (SLC) transporters, and 53 ATP-binding cassette (ABC) transporters and 25 claudin (CLDN) genes.

Gene symbol	Gene name	BBB association
OCLN	occludin	tight junctions
TJP1	tight junction protein 1, ZO1	tight junctions
TJP2	tight junction protein 2, ZO2	tight junctions
TJP3	tight junction protein 3, ZO3	tight junctions
PECAM1	platelet and endothelial cell adhesion molecule 1	tight junctions
CAV1	caveolin 1	associated with BBB permeability
CAV2	caveolin 2	associated with BBB permeability
CDH5	cadherin 5	cell-cell adhesion molecule
F11R	JAM1	regulator of tight junction assembly
FLT1	fms related tyrosine kinase 1, VEGFR1	vascular endothelial growth factor receptor

HIF1A	hypoxia inducible factor 1 alpha subunit	VEGF regulator
ICAM1	intercellular adhesion molecule 1	inflammatory associated factor
ICAM2	intercellular adhesion molecule 2	inflammatory associated factor
ICAM3	intercellular adhesion molecule 3	inflammatory associated factor
ICAM4	intercellular adhesion molecule 4	inflammatory associated factor
F11R	junctional adhesion molecule, JAM1	regulator of tight junction assembly
JAM2	junctional adhesion molecule, 2	localized in tight junctions
JAM3	junctional adhesion molecule, 3	localized in tight junctions
VWF	von Willebrand factor	regulates BBB permeability
VCAM1	vascular cell adhesion molecule 1	mediates leukocyte-endothelial cell adhesion
MCAM	melanoma cell adhesion molecule	regulates T lymphocytes access to the CNS

Supplemental Table 6. Related to Figure 1 and to STAR methods. qRT-PCR Primer sequences.

Primer name	Primer sequence
GAPDH F	GAGTCAACGGATTTGGTCGT
GAPDH R	TTGATTTTGGAGGGATCTCG
KLF9 F	TGGCTGTGGGAAAGTCTATG
KLF9 R	GTCTGAGCGGGAGAACTTTT
HR F	TGGGTCAAGTTTGATATCCGG
HR R	AGGAAGGTTGTGGAGTTGG
MCT8 F	CAACATGCGAGTGTTCCGCCAA
MCT8 R	AAGAGCACCCAGGTCTCCTTGA
MCT10 F	TTGGGCAGCAAAAGAAAATC
MCT10 R	GTGTCCATGCTGGAAACCTT
LAT1 F	ACGCTGTAGCAGTTCACGG
LAT1 R	CTGCTCAAGCCGCTCTTC
LAT2 F	GTGAAGATGTCTTGAACCCG
LAT2 R	GAAGGCAGAGAAGTGAACGC
OATP1C1 F	TCTCTGTTCGGCATGGTGACGT
OATP1C1 R	CACTGCTGGAATGTTGATGAGCC
DIO1 F	TTCAGCACCAGTGGCCTATT
DIO1 R	GTGGTCGTGGGTAAAGTGCT
DIO2 F	GCCACTGTTGTCACCTCCTT
DIO2 R	CCTCCTCGATGCCTACAAAC
DIO3 F	CAGCAGCTCTGCCTAGGACT
DIO3 R	TGAGACTCCTGGGGAATGAC